Robust Intensity-Based Localization Method for Autonomous Driving on Snow-Wet Road Surface

doi: 10.1109/TII.2017.2713836

Robust Intensity Based Localization Method for Autonomous Driving on Snow-wet Road Surface

Mohammad Aldibaja., Naoki Suganuma, and Keisuke Yoneda, *Member, IEEE*

***Abstract*— Autonomous vehicles are being developed rapidly in recent years. In advance implementation stages, many particular problems must be solved to bring this technology into the market place. This paper focuses on the problem of driving in snow and wet road surface environments. First, the quality of LIDAR reflectivity decreases on wet road surfaces. Therefore, an accumulation strategy is designed to increase the density of online LIDAR images. In order enhance the texture of the accumulated images, Principal Component Analysis (PCA) is used to understand the geometrical structures and texture patterns in the map images. The LIDAR images are then reconstructed using the leading principal components with respect to the variance distribution accounted by each eigenvector. Second, the appearance of snow lines deforms the expected road context in LIDAR images. Accordingly, the edge profiles of the LIDAR and map images are extracted to encode the lane lines and roadside edges. Edge matching between the two profiles is then calculated to improve localization in the lateral direction. The proposed method has been tested and evaluated using real data that collected during the winter of 2016/2017 in Suzu and Kanazawa, Japan. The experimental results show that the proposed method increases the robustness of autonomous driving on wet road surfaces, provides a stable performance in laterally localizing the vehicle in the presence of snow lines and significantly reduces the overall localization error at a speed of 60km/h.**

***Index Terms*—Autonomous vehicles, laser imaging detection and ranging (LIDAR), autonomous localization, principal component analysis (PCA), template matching.**

I. Introduction

AUTONOMOUS vehicles have become an important requirement to improve human life quality and safety. In terms of quality, such vehicles can significantly decrease traffic jams and transportation fee; moreover, this facility will be applicable for people regardless age, e.g., handicapped and older people can easily make use this facility. Increasing the safety is an intuitive outcome of bringing autonomous vehicles into reality. Autonomous vehicles are expected to reduce traffic accidents to nearly zero level so that various networks and sharing information can be established and achieved. Various studies have been conducted to create a world model around the vehicle to interpret the sensing information, know what things to concern and plan the movement accordingly [1]. In order to achieve these tasks, numerous complicated operations must be addressed such as localization, mapping, path planning, obstacle detection, traffic-signal recognition and collision prediction [2-5].

Localization and mapping come together as a main requirement to enable autonomous driving. A high definition map is generated to describe the surrounding environment accurately [6]. Localization techniques are then used to precisely localize the vehicle by measuring the similarity between the observation sensing on the environment and the corresponding generated map in the lateral and longitudinal directions. Technically, mapping and localization strategies are designated based on the sensors such as camera or laser imaging detection and ranging (LIDAR). Camera based systems are preferred as they are commercial and simpler [7]. However, laser based systems are currently more reliable because laser beam reflectivity is not influenced by lighting conditions. Moreover, static and dynamic objects can be easily removed based on height information [8]. Thus, laser based systems serve as a basis to switch smoothly to camera based system deployment. This transition strategy is being followed in the unit of autonomous vehicles in Kanazawa University, Japan, to explore, investigate and address many particular and critical problems. One of these problems that observed in 2016 is driving autonomously in snow and wet-ground environments. This problem is often neglected as autonomous driving is usually conducted in good weather conditions. However, such a serious problem cannot be ignored if autonomous vehicles are to be commercialized. The first effect of this problem is that the quality of LIDAR images becomes low because of the weak reflectivity of the wet road surface as illustrated in Fig. 1a. Thus, many regions disappear in the LIDAR image compared to that in the corresponding map image. Moreover, the intensity level of the LIDAR image differs from that of the map image. This explicitly affects the similarity measurement of the static features between the map and the LIDAR images. The second effect is the existence of snow lines inside the lane and near the roadsides. Snow lines form additional like-areas similar to the lane lines as shown in Fig. 1b. These extra areas may dominate the similarity measurement operation and make the vehicle to drift lateral. This situation is particularly dangerous on roads

This Manuscript received November 30, 2016. Received in the revised form April 25, 2017. Accepted for publication May 18, 2017. Copyright 2009 IEEE. This work was supported in part by Ministry of Internal Affairs and Communication under the Strategic Information and Communication R&D Promotion Program (SCOPE) No. 152305001.

Mohammad. Aldibaja., Naoki Suganuma and Keisuke Yoneda are with the Department of Natural Science, Autonomous Vehicle Research Unit, Institute for Frontier Science Initiative, Kanazawa University, Kakuma-Matchi, Kanazawa, Ishikawa 920-1192, japan (Phone: +81-76-234-4714; Fax: +81-76-234-4714; e-mail: suganuma@staff.kanazawa-u.ac.jp)

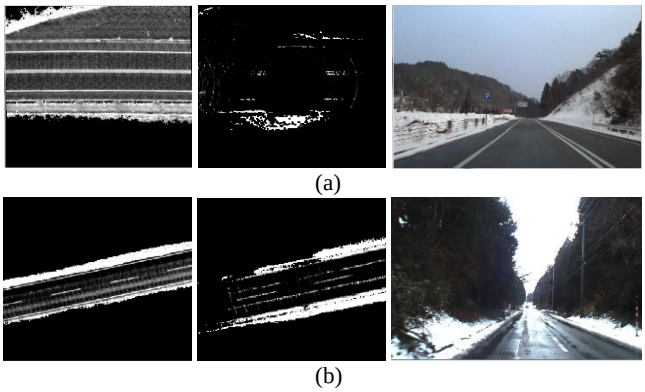

Fig. 1. Localization problems illustrated by map image, corresponding enlarged LIDAR image and camera image. (a) Low LIDAR image quality because of wet ground (b) Deformed road structure due to snow lines inside the lane.

with only two lanes.

The main contributions of this paper are to address the aforementioned issues and propose relevant solutions. As the paper is an extension of our conference paper [9], more details and discussions are provided as well as a new strategy of accumulating LIDAR frames during the autonomous driving is explained. The LIDAR frames are accumulated to enhance the texture and structure of the road representation. Principal Component Analysis (PCA) is employed to reconstruct the accumulated LIDAR image based on the map images. The two unique steps help in improving the quality of the LIDAR image on wet road surfaces by recovering some missing areas and bringing the intensity level to that of the map images. Edge profiles of the LIDAR and map images are then calculated to describe the road structure by a number of picks. The pick distribution helps in encoding the positions of lane lines, roadsides and snow lines. The snow lines appear as extra picks in the LIDAR profile. Therefore, an edge matching strategy is applied to reduce the effects of snow lines and estimate the lateral location of the vehicle based on the common picks between the LIDAR and map profiles.

A localization system along with these improvement steps has been tested using real data. The data were collected in 2016/2017 from the cities of Suzu and Kanazawa, Japan. Snow and rain were frequently observed during the collection phase. We were permitted to conduct autonomous driving at a maximum speed of 60km/h and difficult situations were encountered including the mentioned ones in this paper. The results have verified that the improved localization system is more stable and robust in overcoming the snow line and wet road surface situations.

II. STANDARD LOCALIZATION SYSTEM

Localization techniques are broadly fall into two categories: intensity based and features based [10][11]. In camera based systems, features are generally used because images are rich with different patterns and textures. The features can be extracted from poles, billboards, traffic signs, street indicators, etc. The relevant maps are predefined images that contain various measurements of the features, e.g., position, size, shape, color, etc. Localization is done by minimizing the error between the map information and the actual features that are being extracted from the camera image [12]. On the other hand, a LIDAR image is sparse and less detailed to accurately express particular features at different positions of the vehicle. Therefore, LIDAR based systems are usually designed to use a holistic scanning of the environment and feature extraction can be partially incorporated to support the localization technique [13]. LIDAR maps are generated by accumulating point clouds to precisely describe the environment in 2D or 3D coordinate systems. Localization is achieved by measuring the matching score between the map and LIDAR images. In the next subsections, a brief explanation on a standard LIDAR based localization method is provided with relevant problems and developments. This method was used in the unit of autonomous vehicle in Kanazawa University, 2015/2016.

A. Intensity Based Localization (Image Matching)

GPS data have low accuracy, in the range of 100cm, and cannot be used to localize autonomous vehicles. Moreover and with incorporating Real Time Kinematic (RTK) system, the signals received from satellites are subject to noise. The noise is due to static and dynamic objects depending on the weather and driving conditions. Dead reckoning is usually used to estimate the vehicle location $\mathrm{x}_{t,\mathrm{DR}}$ based on the velocity v and elapsed time series Δt as illustrated in (1).

$$\begin{aligned} &\mathbf{x}_{t,\mathrm{DR}} = \mathbf{x}_{t-1,\mathrm{DR}} + \mathbf{v}_{t-1}\Delta t \\ &\begin{bmatrix} x_{t,\mathrm{DR}} & y_{t,\mathrm{DR}} \end{bmatrix}^{\mathrm{T}} = \begin{bmatrix} x_{t-1,\mathrm{DR}} & y_{t-1,\mathrm{DR}} \end{bmatrix}^{\mathrm{T}} + \begin{bmatrix} v_{t-1}\Delta t & v_{t-1}\Delta t \end{bmatrix}^{\mathrm{T}} \end{aligned} \tag{1}$$

The estimation error is proportional to the distance from the initial position. In order to bring more confidence to this technique and obtain the actual position $\mathrm{x}_{t,\mathrm{Act}}$ accurately, we try to estimate the offset $\Delta \mathrm{x}_{t,\mathrm{DR}}$ between the reference and current environment representations using (2).

$$\begin{aligned} &\mathbf{x}_{t,\mathrm{Act}} = \mathbf{x}_{t,\mathrm{DR}} + \Delta\mathbf{x}_{t,\mathrm{DR}} \\ &\begin{bmatrix} x_{t,\mathrm{Act}} & y_{t,\mathrm{Act}} \end{bmatrix}^{\mathrm{T}} = \begin{bmatrix} x_{t,\mathrm{DR}} & y_{t,\mathrm{DR}} \end{bmatrix}^{\mathrm{T}} + \begin{bmatrix} \Delta x_{t,\mathrm{DR}} & \Delta y_{t,\mathrm{DR}} \end{bmatrix}^{\mathrm{T}} \end{aligned} \tag{2}$$

The reference representation is described by predefining 2D high definition maps using LIDAR point clouds as shown in Fig. 2a. The current environment is represented by online LIDAR image as in Fig. 2b. The localization is then achieved by calculating the cross correlation between the template (LIDAR) and map images as expressed in (3).

$$\begin{aligned} &R_{img}(\Delta x,\Delta y) = \frac{\sum_{i=0}^{N-1}\{m_i(\Delta x,\Delta y)-\overline{m}\}\{z_i-\overline{z}\}}{\sqrt{\sum_{i=0}^{N-1}\{m_i(\Delta x,\Delta y)-\overline{m}\}^2}\sqrt{\sum_{i=0}^{N-1}\{z_i-\overline{z}\}^2}} \\ &\overline{m} = \frac{\sum_{i=0}^{n-1} m_i(\Delta x,\Delta y)}{n} \quad \overline{z} = \frac{\sum_{i=0}^{n-1} z_i}{n} \end{aligned} \tag{3}$$

where $m_i(\Delta x, \Delta y)$ is the expected infrared reflectivity for the map at the offsets $(\Delta x, \Delta y)$, Z represents the infrared reflectivity of the LIDAR image and n is the number of searched positions.

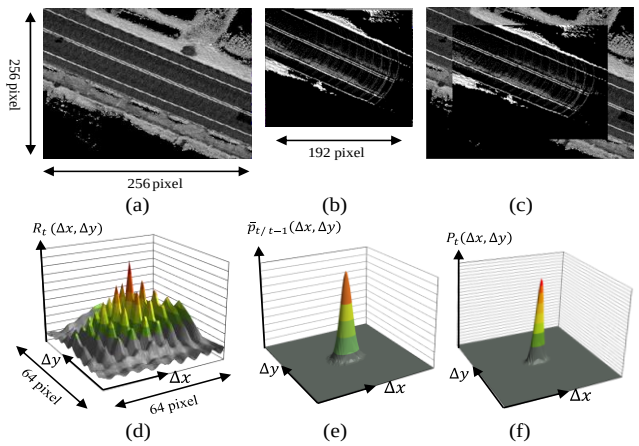

Fig. 2. Localization system. (a) Map image. (b) LIDAR image. (c) Matching image. (d) Image matching distribution. (e) Predicted posterior probability. (f) Current posterior probability.

The equation describes the matching score at each visited position by the template in the map image as illustrated in Fig. 2d. In order to keep modelling the changes in the matching distribution, prior posterior probability $P_{t-1}(i,j)$ is incorporated using (4).

$$\bar{P}_t(\Delta x, \Delta y) = \eta \sum_{i,j} P_{t-1}(i,j) \exp\left(-\frac{(i-\Delta x)^2 + (j-\Delta y)^2}{2\sigma_t^2} \right) \tag{4}$$

where η is the normalizing constant, $\bar{P}_t(\Delta x, \Delta y)$ is the predicted posterior probability of the current vehicle pose and σ_i is the error covariance as shown in Fig. 2e. Finally, the two terms of the predicted and image matching probabilities are multiplied to estimate the current posterior probability $P_t(\Delta x, \Delta y)$ as clarified in (5) and Fig. 2f.

$$P_t(\Delta x, \Delta y) = \eta \cdot \left\{ \left(R_t(\Delta x, \Delta y) + 1 \right)^{\gamma} \bar{P}_t(\Delta x, \Delta y) \right\}^{\beta} \tag{5}$$

where β and γ are constants used to prevent the likelihood distribution from being too smooth. The posterior probability is expected to be sharp and stable such that it can be utilized to calculate the offsets $\Delta x_{t,\mathrm{DR}}$ using (6).

$$\Delta x_{t,\mathrm{DR}} = \frac{\sum_{\Delta x, \Delta y} P_t(\Delta x, \Delta y) \Delta x}{\sum_{\Delta x, \Delta y} P_t(\Delta x, \Delta y)} \quad \Delta y_{t,\mathrm{DR}} = \frac{\sum_{\Delta x, \Delta y} P_t(\Delta x, \Delta y) \Delta y}{\sum_{\Delta x, \Delta y} P_t(\Delta x, \Delta y)} \tag{6}$$

Consequently, (2) is applied and the vehicle position is estimated as illustrated in Fig. 2c, i.e. the LIDAR image overlaps the map image based on the estimated position.

III. Problems and Proposed Improvements

The represented system in the previous section has been evaluated in 2015/2016 in Suzu city, Japan. In winter, we were permitted for the first time in Japan to conduct autonomous driving under very hard weather conditions such as snow, rain and wet-ground environments. Unfortunately, the system performance was very unstable because of the low quality of LIDAR image and the appearance of snow lines. In the next subsections, these two problems are explained in details with corresponding proposed solutions.

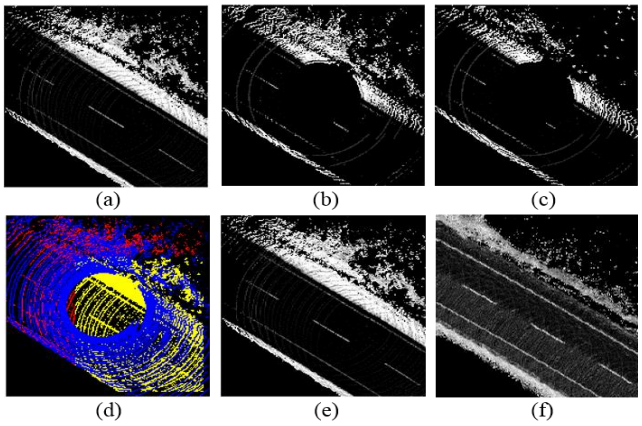

Fig. 3. Online LIDAR frame accumulation. (a) Previous accumulated image. (b) Current frame. (c) Last frame in the stack (must be deleted). (d) Accumulation process: colors blue, yellow and red indicate the current frame, deleted pixels and previous accumulated image pixels, respectively. (e) New accumulated image. (f) Corresponding patch in the predefined map image.

A. Enhancing LIDAR Image Quality by Increasing Density

A LIDAR frame is sparse and cannot be in the same resolution of map images during the autonomous driving because of processing time and vehicle velocity. In order to enhance the real-time environment description, a certain number of frames are accumulated and a stack of the last L frames is created and simultaneously updated. Technically, the LIDAR image is fixed in size and a data association problem must be addressed, i.e., the accumulated LIDAR image is generated as a contribution of the previous accumulated image, shown in Fig. 3a, and the current LIDAR frame in Fig. 3b. Accordingly and before adding the current LIDAR frame, the contribution of the last frame in the stack, Fig. 3c, must be deleted from the previous accumulated image. As the vehicle velocity may change during the L frames, pixel values are deleted with respect to the vehicle pose in the last frame. Therefore, a stack on the vehicle poses in the L frames is also created and updated. This technical operation is applied particularly for each pixel in the new accumulated image because the last frame may share only few pixels (not entire) with the current frame as illustrated in Fig. 3d. Figure 3e demonstrates the above strategy and shows the accumulated LIDAR image. A significant enhancement between the accumulated image and the current frame in Fig. 3b can be observed in terms of appearance, texture and context compared to the corresponding predefined map image in Fig. 3f.

B. Enhancing LIDAR Image Quality Using PCA

The represented system using (5) is sensitive to particular changes in image patterns and textures. LIDAR-based localization systems are ineffective in wet-grounds and rain environments because the reflectivity of the laser beams becomes very weak. Thus, many expected areas in LIDAR

images are distorted compared to the map images. Moreover, the contrast of the snow/wet areas is higher/less than that in the corresponding areas in map images. This increases the effects of the intensity difference in the matching calculation $R(\Delta x, \Delta y)$ and incorrect offsets $\Delta x_{t,\mathrm{DR}}$ are obtained accordingly. In order to improve the system performance and achieve a more robust matching calculation, PCA is employed to reconstruct LIDAR images using map images. This improvement step is performed to recover some missing areas and adjust the intensity level of the LIDAR images to best align the level in the map images.

PCA has been used to solve various problems in image processing including data reduction [14], shape modeling and reconstruction [15], pattern analysis [16], object classification and detection [17] and image reconstruction [18]. The principle is to represent *M* vectors as points in *N* dimensional space. The point distribution in the space increases based on the variance between the vectors. The point distribution can be described efficiently by fitting a new coordinate system, called eigenspace, to maximize the variation encoding. From the view of this paper, eigenspace provides two advantages. First, the directions of the most variations in the *M* vectors can be obtained by the first eigenvectors. Therefore, the noise can be filtered by reconstructing a vector using these few eigenvectors. This step brings the intensity level of the reconstructed vector to that of the *M* vectors. Second, the patterns can be refined by projecting into the eigenspace and adjusting the outrange projections based on the encoded variance in each eigenvector. This step recovers the missing values and approximates wrong patterns to those in the *M* vectors. The above explanation is mathematically translated in the following section.

The map image, shown in Fig. 4a, is divided into *M* blocks with size of *N*×*N*. Each block is converted into N^2 dimensional vectors containing the pixel intensity values. The mean vector $\bar{I}$ is calculated using (7) and the vectors are translated into zero-mean values I' accordingly.

$$\bar{I} = \frac{1}{M}\sum_{i=1}^{M} I_i \qquad I_i^{'} = I_i - \bar{I} \tag{7}$$

The translated vectors are arranged in a matrix Θ and the corresponding covariance matrix *C* is calculated using (8). The covariance matrix expresses the relationships between the pixels of the vectors with respect to their positions.

$$\Theta = [I_i^{'}, I_i^{'}, ..., I_M^{'}]^T \qquad C = \frac{1}{M}\Theta\Theta^T \tag{8}$$

The eigenvectors of the covariance matrix are then computed by solving (9) and the corresponding eigenvalues λ are obtained as shown in Fig. 4b.

$$C\,\Omega = \lambda\,\Omega \tag{9}$$

where Ω is the eigenvector matrix. A vector/block can be restored by a weighting linear combination of the eigenvectors

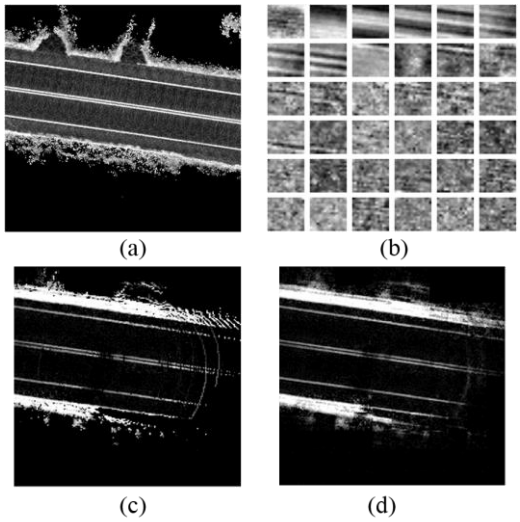

Fig. 4. LIDAR image reconstruction. (a) Map image. (b) Eigenvectors of the map image. (c) LIDAR image. (d) Reconstructed LIDAR image.

using (10). The weights are contained in the projection vector *B* which represent the positions of the projected vector in the eigenspace.

$$I_i = \bar{I} + I_i^{'} = \bar{I} + \Omega B_i \tag{10}$$

Equation (10) is the eigenspace equation which models the patterns and the intensity values in the *M* map blocks (map image).

In order to enhance the online LIDAR image quality in Fig. 4c, the image is divided into *S*<<*M* blocks with size of *N*x*N* and converted into *S* vectors. Each vector is projected into the eigenspace to determine its position using (11).

$$B_i = \Omega^{-1}(I_i - \bar{I}) \tag{11}$$

The position is modified by checking the projections with respect to the corresponding eigenvalue λ_i of each eigenvector. Accordingly, the outrange projections are corrected to be in the range of $\pm 3\sqrt{\lambda_i}$ to obtain a regular Gaussian distribution. The block is then reconstructed using (10) and the corrected projection vector as illustrated in Fig. 4d for the entire blocks. Image matching probability (3) is then calculated between the map and reconstructed LIDAR images.

C. Edge matching for reducing snow line effects

The represented system in (5) has also yielded unstable performance in some situations especially when the matching probability $R_i(\Delta x, \Delta y)$ is continuously incorrect for long distances. Accordingly, the error in the prior probability P_{t-1} is accumulated and a sudden lateral deviation of the vehicle occurs. The main reason behind this scenario is the difference in road patterns between the map images and the actual environmental conditions. Snow lines are formed because of car motions and supposed to appear inside lanes and externally beside lane lines, e.g., the waiting and emergency areas. The

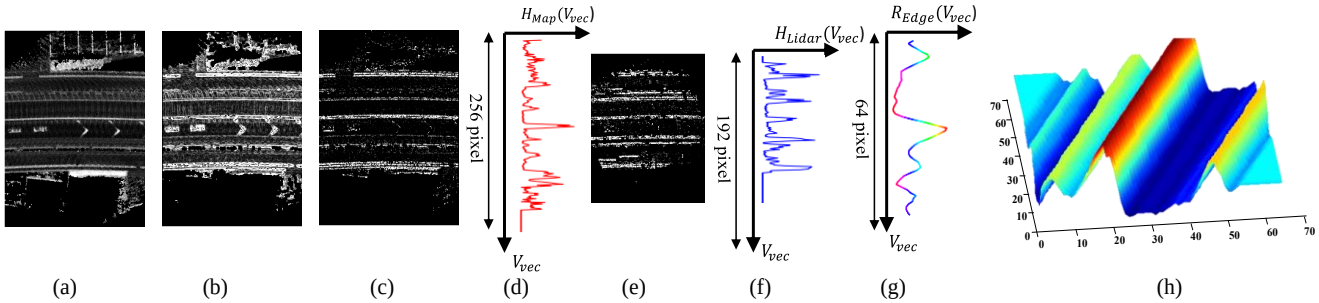

Fig. 5. Edge matching integration. (a) Map image. (b) Strength of gradients. (c) Filtered image based on gradient directions. (d) Map Edge profile. (e) Filtered LIDAR image. (f) LIDAR edge profile. (g) Edge matching profile. (h) Matching profile represented in two directions.

representation of snow lines is similar to the lane lines in LIDAR images as shown in Fig. 1b. These lines deform the expected road pattern and increase the occurrence of similar areas compared to the map image. Consequently, the image matching calculation using (3) may yield a high probability to laterally localize the vehicle towards the snow lines. In order to make the system more robust to the environmental changes, edge matching is incorporated. The lane lines and road edges are more static and are less affected by changing of the environmental conditions. These edge features are extracted by applying Sobel filter on the map and LIDAR images [19]. The strength $E\ (u,v)$ and direction $\theta_E(u,v)$ of the extracted edges are obtained by (12).

$$E(u,v)=\sqrt{E_{\mathrm{U}}^2(u,v)+E_{\mathrm{V}}^2(u,v)}$$
$$\theta_{\mathrm{E}}(u,v)=\arctan\left(E_{\mathrm{V}}(u,v)/E_{\mathrm{U}}(u,v)\right) \quad (12)$$

where E_U and E_V are the gradient components in u and v directions respectively. Figures 5a and 5b show a map image and the corresponding strength of the edges, i.e., the edge image. The edges that are parallel to the vehicle heading direction are very significant for lateral controlling. Thus, the edge image is filtered based on the gradient directions θ_E to encode edges with less than 20deg as illustrated in Fig. 5c. The averaged value H_{Map} in each row v of the filtered image $E'_U(u,v)$ is calculated using (13) with respect to the number of edges $N(v)$.

$$H_{\mathrm{Map}}(v)=\frac{1}{N(v)}\sum_{i=0}^{N(v)-1}E_U^{'}(u,v) \quad (13)$$

Accordingly, the edge profile of the map is created as shown in Fig. 5d and the edge profile $H_{\mathrm{Obs}}(v)$ of the LIDAR image in Fig. 5e is similarly obtained as shown in Fig. 5f. Edge matching $R_{\mathrm{Edge}}(v_c)$ between the map and LIDAR profiles is then computed and normalized by η using (14) to represent the degree of similarity as illustrated in Fig. 5g.

$$R_{\mathrm{Edge}}(v_{\mathrm{C}})=\eta\sum_{v=v_{\mathrm{C}}}^{v_{\mathrm{C}}+H-1}H_{\mathrm{Map}}(v)H_{\mathrm{Obs}}(v) \quad (14)$$

The edge matching profile is a column vector whereas the image matching produced by (3) is a matrix. Therefore, the edge matching profile is typically propagated in a housing matrix $R_{t,\mathrm{Edge}}(\Delta x,\Delta y)$ that contains the same size of $R_{\mathrm{Img}}(\Delta x,\Delta y)$ as demonstrated in Fig. 5h. Based on the conditional independence assumption, the edge matching and the image matching probabilities are combined with the prior probability in (15) to estimate the posterior probability of the vehicle pose. The offsets and the actual pose of the vehicle are then calculated by following the same steps in (6) and (2) respectively.

$$P_{t/t}(\Delta x,\Delta y)=\eta P_{t/t-1}^{\alpha}(\Delta x,\Delta y)R_{t,\mathrm{Image}}^{\beta}(\Delta x,\Delta y)R_{t,\mathrm{Edge}}^{\gamma}(\Delta x,\Delta y) \quad (15)$$

IV. Setup and Platform

Figure 6a shows the operated platform. The vehicle is equipped with many sensors and devices. Velodyne HDL-64E S2 laser range finder LIDAR with 64 separate beams is attached to the vehicle roof. Velodyne spins to generate 3D point clouds to describe the environment around the vehicle. Applonix POS-LV 220 coupled GNSS/IMU is deployed to receive GPS data and measure the velocity, acceleration and rotation angles. A camera system is utilized for image processing and computer vision applications. Twelve omnidirectional radars are distributed on the vehicle body to scan distant areas in range of 180 m. The outputs of the sensors are sent to the central processing unit installed in the trunk. The

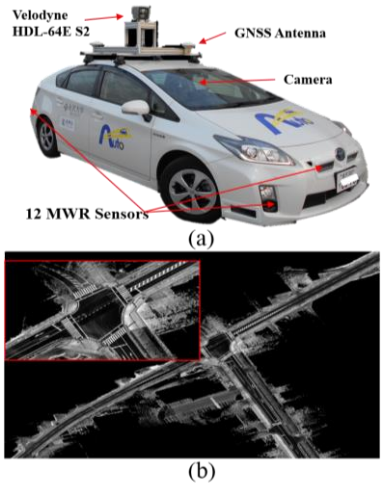

Fig. 6. (a) Operated platform. (b) 2D high definition map.

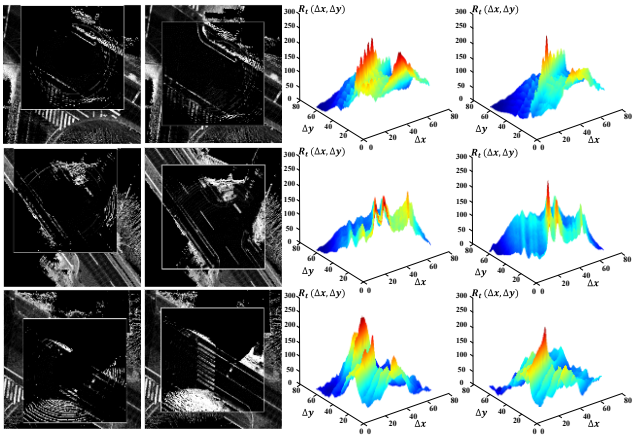

(a) (b) (c) (d)

Fig. 7. LIDAR frame accumulation. (a) Matching result between map image and one LIDAR frame. (b) Matching result using the accumulated LIDAR image. (c) Matching distribution yielded by one frame. (d) Matching distribution yielded by the accumulated image.

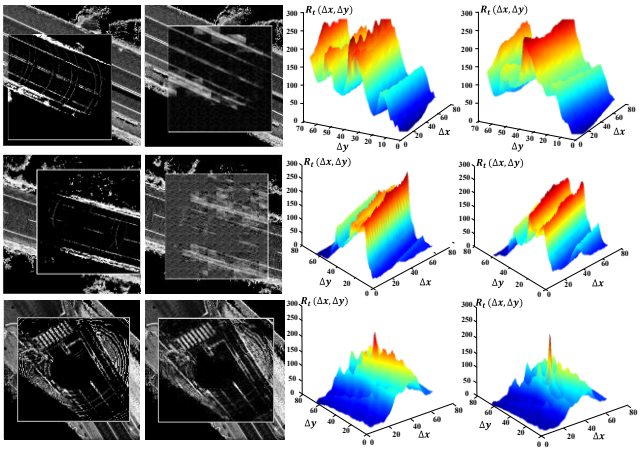

(a) (b) (c) (d)

Fig. 8. LIDAR image reconstruction. (a) Matching result between map image and raw LIDAR image. (b) Matching between map image and reconstructed LIDAR image. (c) Matching distribution yielded by raw image. (d) Matching distribution yielded by the reconstructed image.

processing unit has Intel-Core™ i7-6700 CPU working at 3.40 GH with 8 GB of RAM. The operating system is Windows-7 64X and the localization system was coded using VS-2010 C++ and OpenCV library. The auto-driver comprises many modules such as fusion preceptor, object detection and tracking, traffic signal detection and recognition, path planning, trajectory predictor, localization, mapping and so forth.

The map data were collected by manually driving on roads with good weather conditions in different environments including urban, country side and mountainous regions. The point clouds of LIDAR are accumulated and the dynamic and static objects such as buildings and cars are removed at height of 30cm. The maps were then generated using a post-processing operation to ensure an accurate detail integration. Thus, a 2D map is obtained with encoding the road surface as illustrated in Fig. 6b. The size of each map patch is 64×64 m^2 that represented by 256×256 pixels in the image domain.

The improved system has been tested and evaluated in Suzu and Kanazawa cities, Japan. The maximum speed permitted by the government was 60km/h. The results and images presented in this paper were obtained during the following period: 26th-27th February and 30th-31st March 2016 in Suzu and 27th January and 3rd March 2017 in Kanazawa. The weather in these days was snowing and raining frequently. The road surface was wet and snow covered many areas, i.e., long snow lines appeared in some road segments. Accordingly, various difficult situations were encountered during the autonomous driving. LIDAR data package is sent at a frequency of 10 Hz and GNSS/IMU measurements are obtained with 100 Hz. Therefore, we keep update the vehicle pose using the proposed method in the range of 0.1sec. The online accumulated LIDAR image consists of L=10 frames and covers 32×32 m^2, i.e., 192×192 pixels in the image domain. Obviously, the image matching is calculated 64×64 times and Fourier transform is used to efficiently reduce processing time [20].

LIDAR and map images are divided into blocks with size of 16×16 pixels. The map blocks are used to create the eigenspace that encodes approximately 75% of the total variance. This percent is accommodated by a changeable number k of eigenvectors depending on each map image. We constrain k to be less than 9 because of processing time. However, seven eigenvectors were found sufficient to account the desired variance. LIDAR blocks are projected into the eigenspace and corrected as explained in section III. The GNSS and RTK measurements were stored as ground truth to compare and evaluate the outcomes of the proposed method.

V. Results and Discussion

The online accumulation of LIDAR frames is a unique idea because only a single frame or point cloud is used to localize the vehicle in most of the previous studies [21]. Such an approach provides a sparse representation of the environment. Consequently, the researchers tend to extract some features from the point cloud or to use Iterative Closest Point (ICP) to match the map images [22]. In contrast, the proposed accumulation strategy makes the online LIDAR image dense and more compatible in the intensity level and the appearance with map images. Accordingly, the matching operation becomes more robust in measuring the similarity of the road structures. Figures 7a and 7b illustrate matching results using one LIDAR frame and ten accumulated frames, respectively. The corresponding probability distributions are shown in Figs. 7c and 7d. The matching probability $R(\Delta x, \Delta y)$ indicates better distribution using the accumulated LIDAR image, i.e., the accumulated images correctly overlap the map images and match the road structure based on the position of the maximum matching score in $R(\Delta x, \Delta y)$. This is because of enhancing the road context representation and encoding more details of the environment such as road painting landmarks and surrounding structures.

Figure 8 shows some samples of the image enhancement using PCA. The image matching results to map images using raw and reconstructed LIDAR images are illustrated in Figs. 8a and 8b, respectively. The corresponding matching scores are

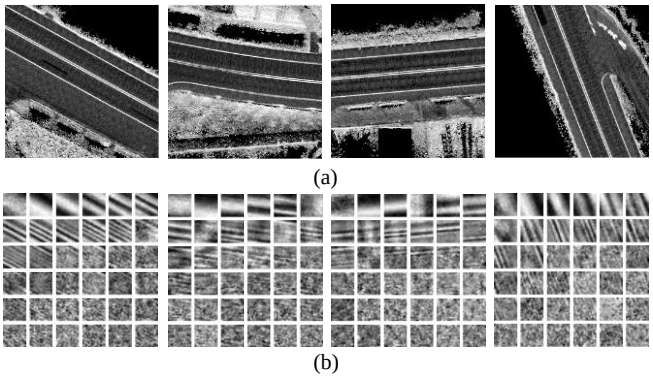

Fig. 9. (a) Map images representing different road structure at different heading angles. (b) Eigenvectors.

shown in Figs. 8c and 8d. The first and second cases in Fig. 8 demonstrate a wrong matching calculation using the raw images because of the wet road surface and the snow appearance at the roadside. The reconstructed images provide correct positions relative to the map images because the intensity level is enhanced and some missing areas with respect to the road context are recovered. The third case shows the same correct matching result that obtained by the raw and reconstructed LIDAR images. On the other hand, the corresponding matching distribution using the reconstructed LIDAR image demonstrates better scores by producing one unique pick whereas multiple picks appear using the raw LIDAR image. These picks are considered noise and they may affect the overall calculation of the posterior probability in (15). Moreover, this case indicates the scalability of the reconstruction strategy to be used commonly when the raw LIDAR image has a good quality.

Covariance matrix C in (8) expresses the relationship between pixels in the blocks. This type of calculation models the geometrical structure and the texture patterns with respect to the pixel positions. As the map images represent only the road surface, these two modeled components dominate the eigenspace. Therefore, the first few eigenvectors are sufficient to express 75% of the total variance in each map image as can be observed in Fig. 4b. Each eigenvalue represents a Gaussian distribution boundary of the encoded features. This provides a generalization capability to the localization system to reconstruct, without any change, the LIDAR blocks that possess legal structure with different textures. Moreover, the reconstructed LIDAR images are ensured to be as similar as possible to the map images in terms of the patterns and intensity level.

Figure 9 emphasizes the previous discussion by showing eigenvectors with corresponding map images. The images represent some road segments with different heading angles and structures. One can observe that the first eigenvectors almost describe the same dominant patterns of the pixel distribution. This indicates the robustness of dividing map images into smaller blocks to encode the curve and straight road segments sufficiently as well as to cover a wide range of environmental changes and reconstruct LIDAR images accordingly.

Figure 10a shows the map image used to create an

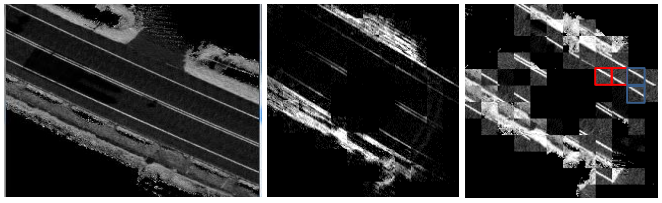

Fig. 10. (a) Map image. (b) Reconstructed LIDAR image. (c) LIDAR image replaced by map blocks. Red rectangles indicate different blocks forming the lane line whereas blue rectangles indicate the same block at different positions.

eigenspace and reconstruct the LIDAR image in Fig. 10b. The reconstructed blocks are replaced by the nearest map blocks in the created eigenspace as illustrated in Fig. 10c. We can emphasize two facts by this image: first, many blocks in the LIDAR image are represented by the same map block. This is because of the generalization capabilities of the eigenspace to distinguish the like-areas in LIDAR images. Second, different map blocks contribute to forming lane lines in the LIDAR image. This indicates the capability of figuring out the map context. Accordingly, the image matching in (3) becomes more robust to the change in the reflectivity of the laser beams on wet road surfaces.

The edge profile provides very significant information to controlling the vehicle laterally. As the map data are usually collected in good weather conditions, the map edge profile is expected to represent the lane lines and road edges with dominant and sharp picks. On the other hand, snow lines create extra picks in the LIDAR profile. Based on the number and the distance between picks in the map profile, the effects of snow can be reduced significantly using (14). From a signal processing viewpoint, the map and LIDAR edge profiles can be considered two signals that share some common properties. The snow lines represented by some picks are considered noise in LIDAR profiles. As common features are expected to dominate the matching calculation, noise appearance (in some range) can be filtered out.

Figure 11 illustrates the effectiveness of incorporating the edge matching calculation in the localization system by demonstrating three instances of the snow formation. Each instance is detailed by showing the front camera image in Fig. 11a, the image matching probability (3) in Fig. 11b, the image matching result in Fig. 11c, the edge matching probability (14) in Fig. 11d, i.e., red represents the map profile, blue represents the LIDAR profile and multiple colors represent the matching profile, and the edge matching result in Fig. 11e. The first case illustrates the snow accumulation at the roadside with a freezing layer on the road surface. This layer influences the LIDAR reflectivity and increases the intensity level. Consequently, the image matching result produces a lateral shifting around 3 meters whereas the edge matching recovers this situation at 12cm. The second case shows a wet road surface with snow segments just beside the lane line. These segments change the road pattern and result in matching the side lane line with the middle line in the map image. In contrast, this situation is also recovered using the edge matching. The third case shows accumulated snow segments at the roadside

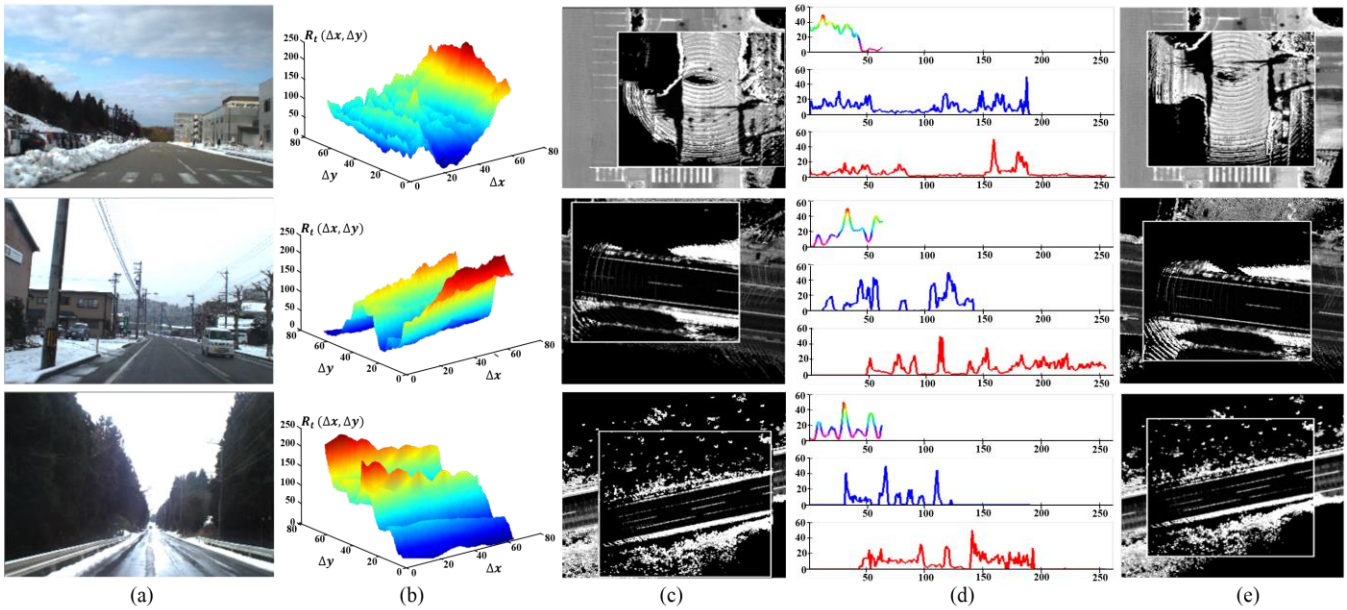

Fig. 11. Edge matching effects. (a) Camera image. (b) Image matching probability. (c) Image matching results. (d) Edge process: red represents map profile, blue represents LIDAR profile and colorful represents matching profile. (d) Edge matching results.

and two snow lines inside the lane. The snow lines influence the image matching result with a considerable lateral shifting. These lines are represented by two noise picks in the LIDAR profile (blue) in Fig. 11d. The effects are eliminated by calculating the edge matching based on the common picks of the lane lines between the LIDAR and map profiles. Accordingly, the edge matching correctly localizes the vehicle as shown in Fig. 11e.

Figure 12 shows a critical situation that occurred on 1st March 2016 because of the snow line existence. The vehicle was pulled two times towards the snow lines near the roadside barrier. The lateral error is approximately 1.2m using the old system (5) whereas it has been reduced significantly to 14cm using the improved system (15). Therefore, the improvement steps have increased the stability and smoothness of the localization system.

As the immediate effects of snow lines and wet road surface are to shift the vehicle laterally, one can infer that the proposed improvements have also enhanced significantly the localization accuracy in the longitudinal direction. Furthermore, the improved system has shown an impressive performance against the environmental changes. Figure 13 highlights an example on changing a grass and vegetation area in Figs. 13a and 13b into a paved land in Fig. 13c. The old system has yielded a wrong lateral estimation in the opposite lane as indicated in Fig. 13d whereas the improved system estimates the vehicle pose accurately as illustrated in Fig. 13e. The error profiles of both the systems along this area are shown in Fig. 13f. This indicates the scalability of the improved system to work robustly in various environments with different weather conditions.

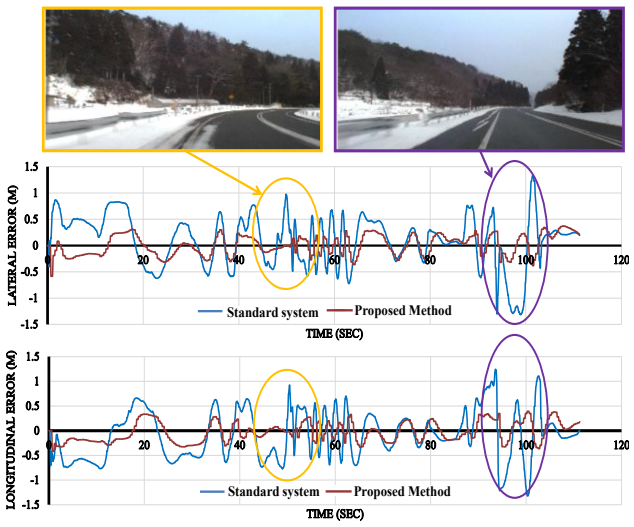

Fig. 12. Localization performances using old and improved systems in snow environment.

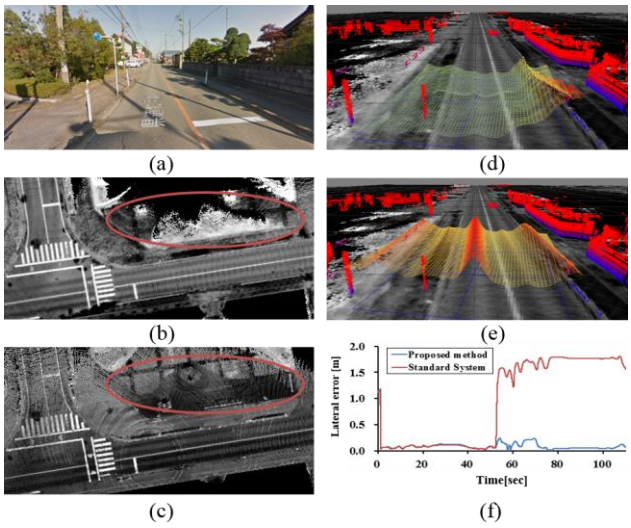

Fig. 13. Old and improved performances against environment changes. (a) Front camera. (b) Grass area. (c) Paved area. (d) Image matching probability. (e) Edge matching probability. (f) Lateral error profiles.

In the overall assessment, the improved system has performed lateral localization error of 20cm in an average of many hard situations of driving autonomously in snow environments and on wet road surfaces. Furthermore, the lateral error is less than 15cm on normal days with good weather conditions. Accordingly, the system is very compatible and robust to be used for autonomous driving under different environmental conditions.

VI. CONCLUSION

This paper focuses on the problem of autonomous driving in wet and snow environments using a probabilistic approach. The density of the online LIDAR image is increased using a frame accumulation strategy. This unique idea has enabled image matching to be more robust by enhancing the representation of the road structure and context. PCA is used to reconstruct LIDAR images by improving the image quality and recovering the missing areas due to the weak reflectivity of LIDAR on the wet road surfaces. Two conditions must be met to reconstruct LIDAR images properly. First, the reconstruction must retain the structure patterns of the unaffected regions with enhancing the intensity level. Second, the missing regions must be recovered with respect to the map context. PCA has satisfied these two conditions by creating an eigenspace that models the map structure and pixel distribution. The generalization capability of this space has provided a better interpretation of the map features. In addition, an edge matching technique is incorporated to increase the robustness of localizing the vehicle in the lateral direction. Edge profile was designed to encode most important features to provide a stable performance against the snow line existence. The effects of snow lines were reduced by filtering out their picks in the edge profile based on the number and distance between the picks in the map edge profile. Moreover, edge matching was proven to recover the matching error when the image matching fails to localize the vehicle. The lateral error obtained by the proposed method is approximately 20cm at a speed of 60km/h. This error is reliable in conducting autonomous driving under hard weather conditions.

REFERENCES

[1] J. Levinson, J. Askeland, J. Becker, J. Dolson, D. Held, S. Kammel, and S. Thrun, "Towards fully autonomous driving: Systems and algorithms", *Proc. IEEE IV*, pp. 163-168, 2011.

[2] J. Levinson, M. Montemerlo, and S. Thrun, "Map-Based Precision Vehicle Localization in Urban Environments," *in proceeding of Robotics Science and Systems*, 2007.

[3] J. Levinson, J. Askeland, J. Dolson and S. Thrun, "Traffic light mapping, localization, and state detection for autonomous vehicles," *in Proceedings of IEEE Conference on robotics and automation*, pp. 5784-5791, 2011.

[4] S. Thrun and M. Montemerlo, "The graph SLAM algorithm with applications to large-scale mapping of urban structures," The International Journal of Robotics Research, vol. 25, no. 5-6, p. 403, 2006.

[5] K. Yoneda, N. Suganuma and M. Aldibaja, "Simultaneous State Recognition for Multiple Traffic Signals on Urban Road" *in Proceedings of MECATRONICS-REM*, pp.135-140, 2016.

[6] J. Levinson and S. Thrun, "Robust vehicle localization in urban environments using probabilistic maps", *in Proceedings of IEEE Conference on robotics and automation*, pp. 4372-4378, 2010.

[7] J. Ziegler, H. Lategahn, M. Schreiber, C. G. Keller, C. Knoppel, J. Hipp, M. Haueis and C. Stiller, "Video based localization for bertha", *Intelligent Vehicles Symposium Proceedings*, pp. 1231-1238, 2014.

[8] N. Suganuma, K. Yoneda and D. Yamamoto, "Localization for Autonomous Driving on Urban Roads", Journal of Advanced Control, Automation and Robotics, vol. 1, no. 1, pp. 47-53, 2015.

[9] M. Aldibaja, N. Suganuma, and K. Yoneda, "Improving localization accuracy for autonomous driving in snow-rain environments," *IEEE/SICE International Symposium on System Integration*, pp. 212-217, 2016.

[10] S. Sivaraman and M. Trivedi, "Looking at vehicles on the road: A survey of vision-based vehicle detection, tracking, and behavior analsis", IEEE Trans. Intelligent Transportation Systems, vol. 14, pp. 1773-1795, 2013.

[11] N. Mattern and G. Wanielik, "Vehicle localization in urban environments using feature maps and aerial images", *in Proceedings of IEEE Conference on Intelligent Transportation System*., pp. 1027-1032, 2011.

[12] O. Pink, "Visual map matching and localization using a global feature map," *in IEEE Computer Vision and Pattern Recognition Workshops*, pp. 1-7, 2008.

[13] Y. Li and E. B. Olson, "Extracting general-purpose features from lidar data," in Robotics and Automation, 2010. Proceedings. ICRA '10. 2010.

[14] E. Jackson A User's Guide to Principal Components, 1-25, 1999.

[15] M. Aldibaja, and S. Suzuki, "Eye Features Extraction Based on Eye Color Interpretation in Eigenspace and Eye Structure Representation in Logarithmic-Polar Domain", Journal of Japan Society of Mechanical Engineering, vol. 14, pp. 264-271, 2014.

[16] M. Turk and A.P. Pentland, "Face Recognition Using Eigenfaces," *IEEE Conf. Computer Vision and Pattern Recognition*, pp. 586-591, 1991.

[17] A. Abadpoura and S. Kasaeib, "An efficient PCA-based color transfer method," Journal of Visual Communication and Image Representation, Vol. 18, Issue 1, pp. 15-34, 2007.

[18] L. M, Borja, O. Fuentes J.D. Foley, "Object detection using image reconstruction, with PCA", Image and Vision Computing 27, pp. 2-9, 2009.

[19] O. R. Vincent, O. Folorunso, "A descriptive algorithm for sobel image edge detection", *Proc. Inform. Sci. Inform. Tech. Educ. Conf.*, pp. 97-107, Jun. 2009.

[20] A. J. H. Hii, C. E. Hann, J. G. Chase, E. E. W. Van Houten, "Fast normalized cross correlation for motion tracking using basis functions", Comput. Methods Programs Biomed, vol. 82, no. 2, pp. 144-156, 2006.

[21] A. Hata and D. Wolf, "Road marker detection using LIDAR reflective intensity data and its application to vehicle localization," *IEEE International Conference on Intelligent Transportation Systems*, pp. 584-589, 2014.

[22] F. Pomerleau, F. Colas, R. Siegwart, S. Magnenat, "Comparing ICP variants on real-world data sets", Autonomous Robots, vol. 34, no. 3, pp. 133-148, 2013.

Mohammad Aldibaja received his BSc degree from Tishreen University, Latakia, Syria in 2006 and his ME and PhD degrees from Toyohashi University of Technology, Toyohashi, Japan in 2011 and 2015. He is a Postdoctoral Researcher at autonomous vehicle unit in Kanazawa University, Ishikawa, Japan and responsible for LIDAR-based mapping and localization systems. His research interests are computer vision, human machine interface systems and autonomous vehicles.

Naoki Suganuma is with Kanazawa University, Ishikawa, Japan scince 2002 and has received his BE, ME and PhD degrees from this university in 1998, 2000 and 2002. Since 2015 and among Japanese Universities, he started the first public road experiment of Self-driving vehicle on City Street. Currently, he is Associate Professor and the leader of Autonomous Vehi cle research unit, Institute for Frontier Science Initiative, Kanazawa University.

Keisuke Yoneda (M' 2014) received his B.S. degrees in engineering from Toyohashi University of Technology in 2007 and his ME PhD degrees in information science from Hokkaido University in 2009 and 2012. Currently, he is Assistant Professor at Autonomous Vehicle research unit of Institute for Frontier Science Initiative, Kanazawa University. His research interests are autonomous vehicles, artificial intelligence, and artificial life. He is a member of IEEE and the Society of Automotive Engineers of Japan, Inc.